



# Chemistry A European Journal

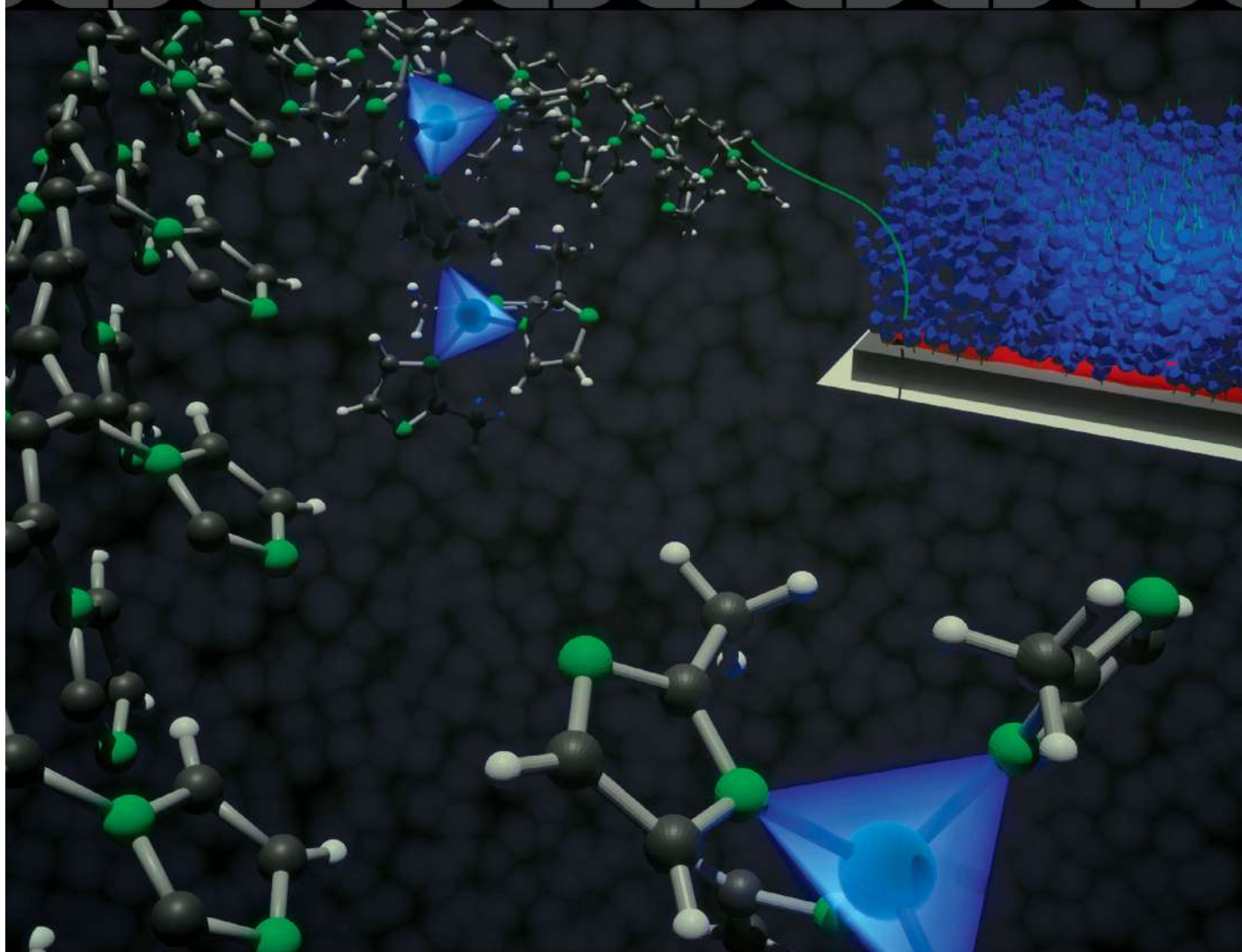


European Chemical  
Societies Publishing

**Cover Feature:**

*O. Azzaroni, M. Rafti et al.*

Growth of ZIF-8 MOF Films with Tunable Porosity by using Poly (1-vinylimidazole) Brushes as 3D Primers



00/2020

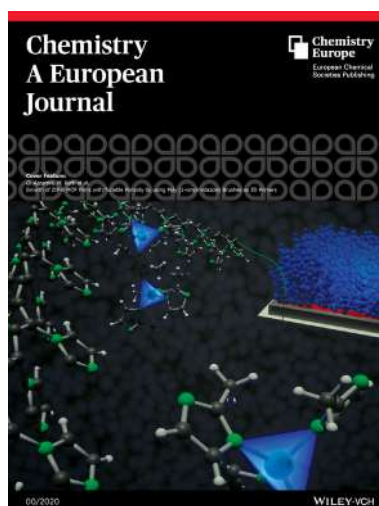
WILEY-VCH

## COVER PICTURE

*J. A. Allegretto, A. Iborra, J. M. Giusti,  
C. von Bilderling, M. Ceolín, S. Moya,  
O. Azzaroni,\* M. Rafti\**



**Growth of ZIF-8 MOF Films with  
Tunable Porosity by using Poly (1-  
vinylimidazole) Brushes as 3D Primers**



**ZIF-8 (based on Zn and 2-methylimidazole)** MOF film growth can be controlled by using SI-ATRP-synthesized polymeric brushes as 3D primers. This strategy relies on the inclusion of chemical moieties in the brush, which are compatible with MOF chemical structure. According to such criteria, Poly(1-vinylimidazole) brushes with increasingly higher grafting densities were selected. Aside from the inherently hydrophobic microporosity arising from ZIF-8 structure, our approach renders control over the proportion of constructional mesoporosity, which allow differential adsorption. More information can be found in the Full Paper by O. Azzaroni, M. Rafti, et al. (DOI: 10.1002/chem.202002493).

## ■ Porous Materials

## Growth of ZIF-8 MOF Films with Tunable Porosity by using Poly (1-vinylimidazole) Brushes as 3D Primers

Juan A. Allegretto<sup>+, [a, b]</sup> Agustín Iborra<sup>+, [a]</sup> Juan M. Giussi,<sup>[a]</sup> Catalina von Bilderling,<sup>[a, c]</sup> Marcelo Ceolín,<sup>[a]</sup> Sergio Moya,<sup>[d]</sup> Omar Azzaroni,<sup>\*[a]</sup> and Matias Rafti<sup>\*[a]</sup>

**Abstract:** This work reports on a novel and versatile approach to control the structure of metal–organic framework (MOFs) films by using polymeric brushes as 3D primers, suitable for triggering heterogeneous MOF nucleation. As a proof-of-concept, this work explores the use of poly(1-vinylimidazole) brushes primer obtained via surface-initiated atom transfer radical polymerization (SI-ATRP) for the synthesis of Zn-based ZIF-8 MOF films. By modifying the grafting density of the brushes, smooth porous films were obtained featuring

inherently hydrophobic microporosity arising from ZIF-8 structure, and an additional constructional interparticle mesoporosity, which can be employed for differential adsorption of targeted adsorbates. It was found that the grafting density modulates the constructional porosity of the films obtained; higher grafting densities result in more compact structures, while lower grafting density generates increasingly inhomogeneous films with a higher proportion of interparticle constructional porosity.

## Introduction

The quest for novel and efficient strategies aimed at obtaining composite porous materials with tailored functional properties remains a very active research sub-topic in materials science.<sup>[1]</sup> Moreover, the ability to synthesize composites featuring porosity with different chemical characteristics adds an additional degree of complexity and greatly enhances the number of possible applications in diverse fields, such as adsorption, catalysis, and energy storage/conversion.<sup>[2–5]</sup>

Appealing examples of such composites are those that include a relatively new class of materials with permanent poros-

ity known as metal–organic frameworks (MOFs), that can be best described as crystalline networks of metal ions (or metal-ion containing clusters) non-covalently bonded to multidentate organic linkers. MOFs can feature remarkably high BET surface areas (up to 6500 m<sup>2</sup>g<sup>−1</sup>, among the highest reported values to date),<sup>[6]</sup> and very versatile surface chemistry, just to mention the key features that have attracted the attention of the materials science research community.<sup>[7–9]</sup>

MOFs can be produced as colloidal dispersions and subsequently used as units for film assembly, or via direct heterogeneous nucleation on suitable substrates. In either case, chemical modification protocols can be applied in order to confer diverse functionalities; e.g., to endow tailored affinity towards selected adsorbates or enhanced hydrophilic/hydrophobic character, thus widening the applications possible.<sup>[10–15]</sup> Among the various available methods for synthesis of MOF films, the Liquid Phase Epitaxy (LPE) is the most suitable because it enables integration into “soft” polymeric composites due to the mild conditions employed.<sup>[16]</sup> Depending on the thickness, two main categories of films can be distinguished; namely, surface mounted MOFs or SURMOFs (few nanometers thick, and usually grown via Langmuir–Blodgett method),<sup>[17]</sup> and MOF thin films (several hundred nanometers thick). Fabrication of such films over desired substrates involves the use of suitable primers that must guarantee mechanical stability and can; e.g., determine a preferred film crystalline orientation or morphology.<sup>[18–23]</sup> Among the most interesting examples of the use of MOF thin films applications in separation membranes,<sup>[24]</sup> electrocatalysis,<sup>[25]</sup> or sensing can be mentioned.<sup>[26–28]</sup>

Polymer-MOF composites are a relatively recent development, with the appealing possibility of further control over structure gained through polymer incorporation. Remarkable examples of possible applications of such composites are the

[a] J. A. Allegretto,<sup>+</sup> A. Iborra,<sup>+</sup> Dr. J. M. Giussi, Dr. C. von Bilderling, Dr. M. Ceolín, Dr. O. Azzaroni, Dr. M. Rafti  
Instituto de Investigaciones Fisicoquímicas Teóricas y Aplicadas (INIFTA), Departamento de Química, Facultad de Ciencias Exactas, Universidad Nacional de La Plata  
CONICET  
Calle 64 y Diag. 113, 1900 La Plata (Argentina)  
E-mail: azzaroni@inifta.unlp.edu.ar  
mrafti@inifta.unlp.edu.ar

[b] J. A. Allegretto<sup>+</sup>  
Universidad Nacional de San Martín (UNSAM)  
San Martín (Argentina)

[c] Dr. C. von Bilderling  
Departamento de Física, Facultad de Ciencias Exactas y Naturales  
Universidad de Buenos Aires  
C1428EHA Buenos Aires (Argentina)

[d] Dr. S. Moya  
Center for Cooperative Research in Biomaterials (CIC biomaGUNE), Basque Research and Technology Alliance (BRTA)  
Paseo de Miramón 182 C, Donostia-San Sebastián, 20014 (Spain)

[\*] These authors contributed equally to this work.

 Supporting information and the ORCID identification number(s) for the author(s) of this article can be found under:  
<https://doi.org/10.1002/chem.202002493>

Mixed Matrix Membranes, in which the MOF-phase is embedded into a polymeric continuous matrix. These architectures can outperform traditional adsorbents for selective transport of gas molecules in technologically-relevant mixtures.<sup>[29,30]</sup> Another important example of polymer-MOF composites was introduced by combining conductive polymers and MOFs into cost-effective composite electrocatalysts.<sup>[31,32]</sup>

Among MOF-based structures, polymer-MOF composite films have the unique advantage of featuring two different classes of environments; i.e., an intrinsic microporosity with uniform size provided by MOF crystalline structure (intraparticle), and an interparticle porosity with somehow high polydispersity and highly dependent on the nature of the polymeric environment (or matrix), also called “constructional” porosity.<sup>[33]</sup>

There are multiple strategies for the integration of polymers and MOFs, which of course render different composite structures. For instance, polymer-embedded MOFs (also known as polyMOFs) can be obtained by incorporating suitable polymers displaying moieties capable of coordinating MOF metallic ions into the synthesis mixtures, or by including monomers in the reaction mixture.<sup>[34]</sup> Spray-drying methods with adequate solvents allow for rapid one-step integration yielding polymer-coated MOFs.<sup>[35]</sup> A large variety of core-shell composites can also be produced by means of surface-initiated atom-transfer radical polymerization (SI-ATRP) reactions.<sup>[36–38]</sup> SI-ATRP usually relies on the presence of amino moieties on the MOF surface, which serve as anchor for covalent binding of the polymerization initiator. Non-covalent positioning (e.g., hydrogen bond crosslinking of carboxylic moieties) of the initiator has also shown to be a valid alternative.<sup>[39]</sup>

The discussed examples strongly rely on interactions between dispersed MOF units and polymers, these approaches restrict somehow the control of resulting composite structure in terms of, e.g., composition and homogeneity. It was already demonstrated that such ability to control composite structure has an important impact on the performance of micro- and nano-structured systems.<sup>[40]</sup> An illustrative example of a different approach is the use of specific interactions between  $\text{Zn}^{2+}$  ions and sulfonate moieties as directing agents for the control of hybrid membranes featuring well-dispersed ZIF-8 MOF units across a poly(4-styrenesulfonic acid) polymeric film. Such composite membrane was shown to be highly homogeneous and mechanically stable with good performances in separation applications.<sup>[41]</sup> The key idea behind this approach is the use of specific interactions between MOFs precursors and targeted polymeric components, which in turn will trigger confined nucleation, as was recently reported for the directed nucleation of ZIF-8 films over Self-Assembled Monolayers (SAMs) exposing appropriate chemical moieties.<sup>[22]</sup> This concept can be further extended to three-dimensions (thus creating a “primer volume”, rather than 2D-SAMs primer surface), by using polymer brushes exposing such moieties responsible for triggering MOF nucleation.<sup>[42]</sup> Polymer brushes allow additional control of the resulting structure by manipulation of variables such as surface grafting density, grafting thickness and spacing of monomers across the polymeric chain.<sup>[43]</sup> By controlling such

parameters, rough assemblies of MOF particles with diameters ranging from 0.09 to 1.3  $\mu\text{m}$  were formed.

The above mentioned Zn-based ZIF-8 MOF belongs to the so called ZIFs subclass (Zeolitic Imidazolate Frameworks), and is one of the most robust and versatile members of the family, and thus one of the most explored for multiple applications. ZIFs subclass features tetrahedrally coordinated  $\text{M}^{2+}$  centers (most commonly zinc and cobalt based) with imidazolate-derived *N*-bidentate linkers. In particular, ZIF-8 features a crystalline sodalite-like topology of  $\text{Zn}^{2+}$  ions coordinated by 2-methylimidazolate ( $\text{mIm}^-$ ) linkers.<sup>[44,45]</sup> ZIF-8 features highly hydrophobic micropores (6 Å pore window, and 11.4 Å diameter) and reported BET surface areas = 1600  $\text{m}^2\text{g}^{-1}$ . The synthesis of ZIF-8 thin films and the control of porous environments are of great interest due to the extensive range of demonstrated applications ranging from gas separation,<sup>[46]</sup> to drug delivery,<sup>[47]</sup> Fabry-Perot devices,<sup>[48]</sup> low-k dielectric materials,<sup>[49]</sup> and various functional composites.<sup>[50]</sup> The highly hydrophobic nature of micropores, which is responsible for its great stability towards hydrolysis, is also a drawback for some intended use because restricts the available contact area necessary for separation purposes.

Inspired by the discussed strategies oriented to the development of complex MOF-polymer architectures with different tailored properties, we took the paradigm one step further and explored the effect of poly(1-vinylimidazole) brushes as 3D primers for ZIF-8 film growth. By selecting this particular monomer with the same chemical moiety than ZIF-8 imidazolate linkers, we aimed to the creation of sites for  $\text{Zn}^{2+}$  positioning, causing confined triggering of ZIF-8 growth.<sup>[51]</sup> In this way, an enhanced integration of the brush monomers into the MOF film could be achieved, together with an improvement in the control over film structure. The results obtained show that brush grafting density used dictates the resulting porous structure of films synthesized; i.e., different brush densities control the proportion of additional constructional mesoporosity, featuring an increased hydrophilic character, which opens the path for the synthesis of films with tailored hydrophilic/hydrophobic adsorption sites.

## Results and Discussion

### Synthesis of ZIF-8@PvIm brushes

The mechanism for the observed ZIF-8 heterogeneous nucleation enhancement can be hypothesized to arise from  $\text{Zn}^{2+}$  pre-concentration in the polymeric primer triggered by coordination imidazole moieties. To bring evidence to the proposed mechanism, a poly(1-vinylimidazole) polymer was synthesized in bulk using identical conditions to those for the brush and characterized by NMR (see section S2.1 in Supporting Information). Then, FTIR spectra obtained for both, as synthesized polymer before and after exposure to  $\text{Zn}^{2+}$  evidences the interaction between  $\text{Zn}^{2+}$  and imidazole thus.

XPS spectra shown in Figures S3 (see Supporting Information) confirm successful surface silanization of silicon substrates, followed by modification of APTES with Br-*i*BuBr initia-

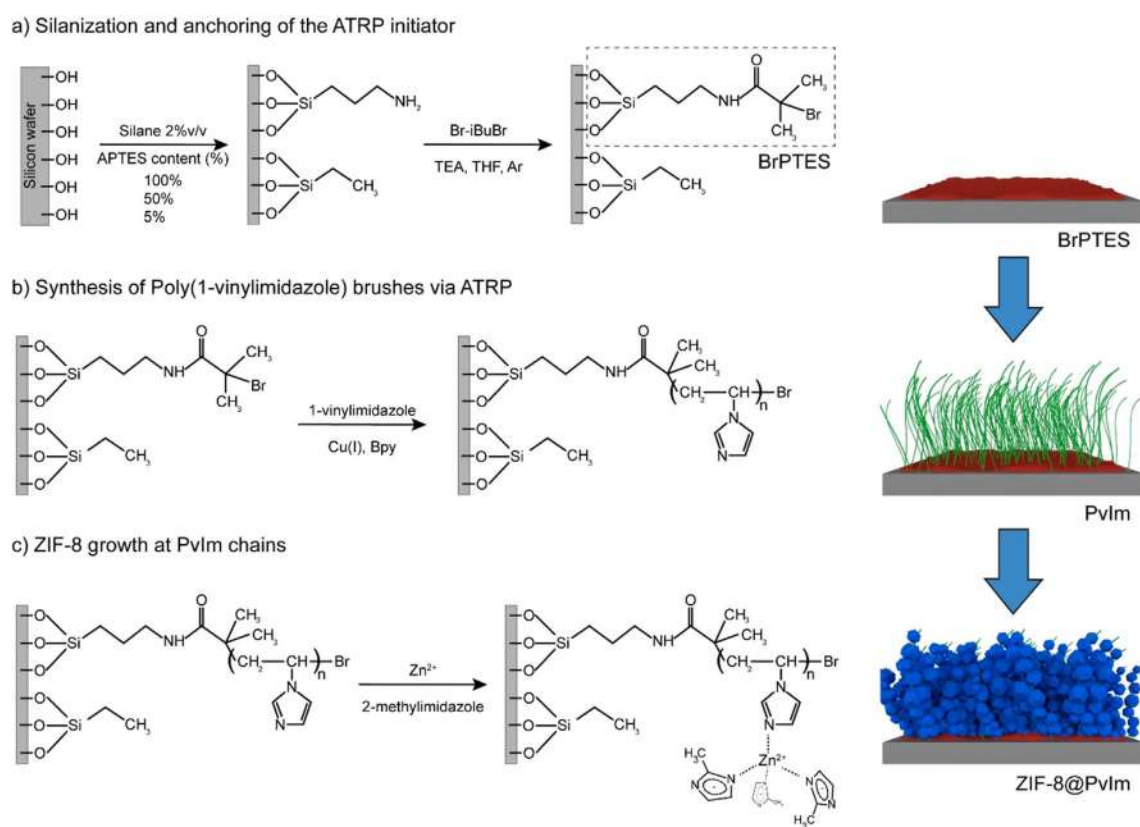
tor. Specifically; this can be inferred from the presence of 287.1 eV binding energy (BE) signal corresponding to C–Br.<sup>[52]</sup> It was observed that XPS-determined Br content decreased as lower APTES percentages were used in the silanization mixture since Br-*i*BuBr modification can only occur when –NH<sub>2</sub> moieties are present (see Supporting Information, Figure S4). By using different APTES proportions, the effective grafting density can be successfully controlled, as summarized in Table 1.

As discussed above and depicted in Scheme 1, brush synthesis and ZIF-8 MOF formation can be followed by looking at changes in the N1s XPS signal. When comparing results obtained for APTES-terminated surface and after Br-*i*BuBr reaction (Figure 1a vs. 1b), an evident shift N1s signal to lower BE occurs. Such an effect can be ascribed to amide tautomeric equilibrium. The appearance of N=C and N–C signals at 398.6 eV and 400.4 eV respectively, confirm the successful syn-

thesis of polymer chains after ATRP reaction (Figure 1c).<sup>[53]</sup> Finally, after ZIF-8 growth, the XPS signal for the N1s region is dominated by 2-methylimidazole present in MOF structure (Figure 1d).<sup>[54]</sup> The discussed sequential changes were also observed when carrying silanization procedure using different APTES percentages (see Supporting Information, Figure S5, together with further details on XPS characterization in Section S2.2). In the supplementary video provided, the proposed mechanism for obtaining the films using the pre-concentration of Zn<sup>2+</sup> by brushes is illustrated with a sketch animation (see Supporting Information, Video 1).

Crystalline structure of the synthesized ZIF-8 films was characterized by XRD. Results are presented in Figure 2a. Even though the positions of diffraction peaks for the synthesized films are in line with the calculated diffractogram from reported ZIF-8 structure, peak width suggests low size crystalline domains. In order to quantify the effect of polymer brush grafting density on film growth, in situ QCM experiments were also carried out on modified sensors. Increasingly higher values for surface mass density ( $\Gamma$ ) can be associated with higher grafting densities as expected from the increasing APTES content in the corresponding silanization mixture used, as observed in Figure 2b. Calculations for  $\Gamma$  were conducted using the Sauerbrey equation, which can be applied due to the low dissipation values obtained ( $8\text{--}15 \times 10^{-6}$  range, 3rd resonator overtone) and the obtained values for the ratio between dissipation and frequency, which allows considering the film as a non-visco-

XPS quantification	APTES content in the silanization mixture [%]		
	100	50	5
C [%]	52.1	43.9	32.8
N [%]	7.2	6.6	3.1
O [%]	39.5	48.5	63.7
Br [%]	1.2	0.9	0.5



**Scheme 1.** Schematized procedure for sequential ZIF-8@PvIm film synthesis: (a) Si wafer surface silanization and anchoring of ATRP initiator, (b) ATRP synthesis of Poly(1-vinylimidazole) brushes, and (c) early stages of heterogeneous nucleation and growth of ZIF-8 films.

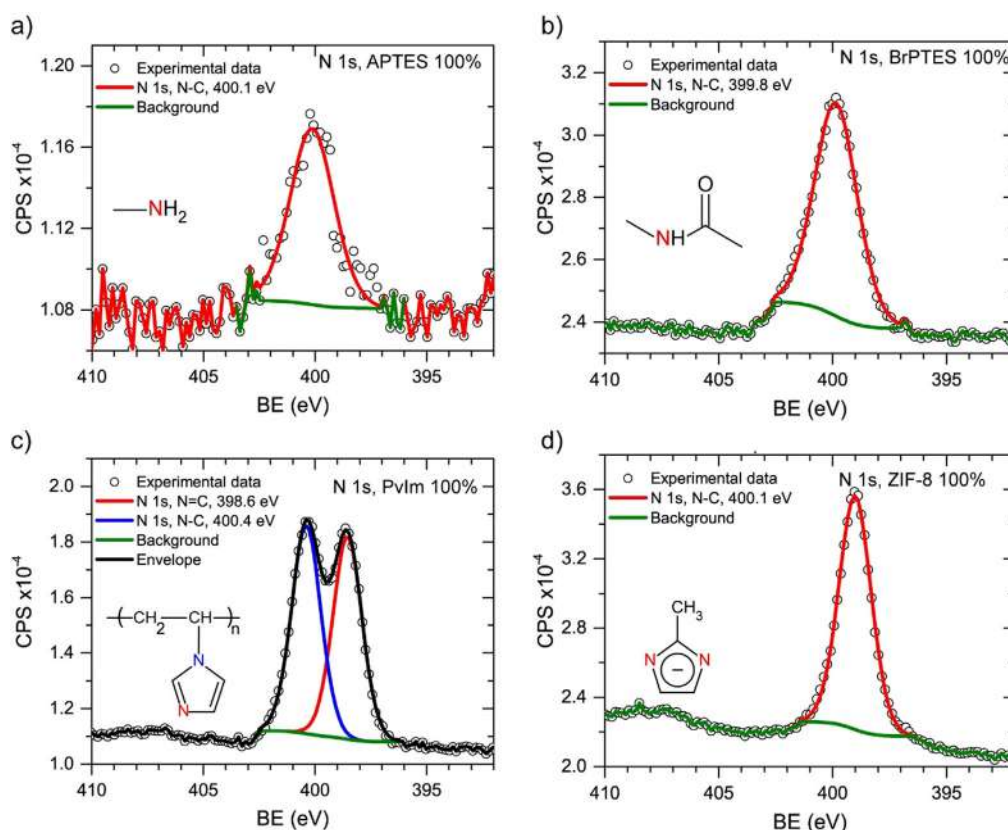


**Figure 1.** XPS N 1s band for each step of the film synthesis. (a) APTES modified substrate, (b) after reaction with Br-*i*BuBr, (c) after ATRP synthesis of PvIm polymeric brushes, and (d) after ZIF-8 synthesis on PvIm (ZIF-8@PvIm).

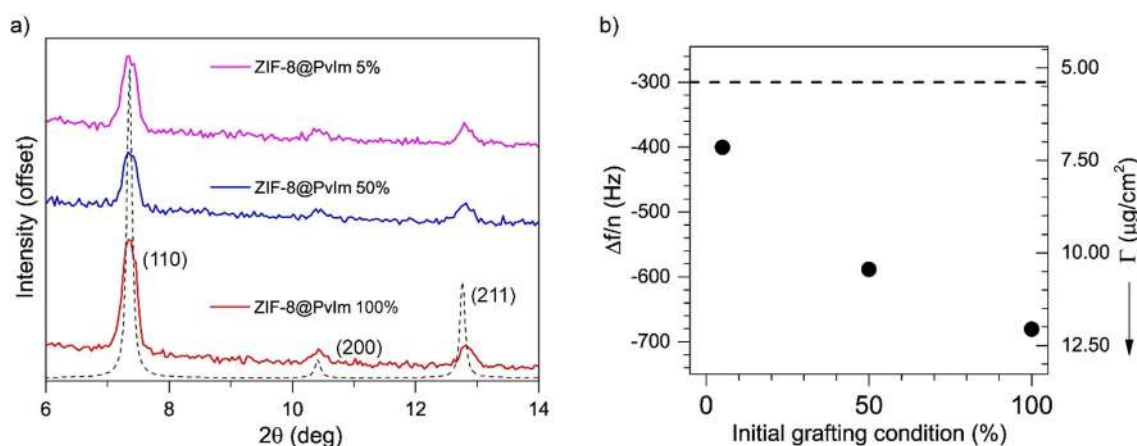


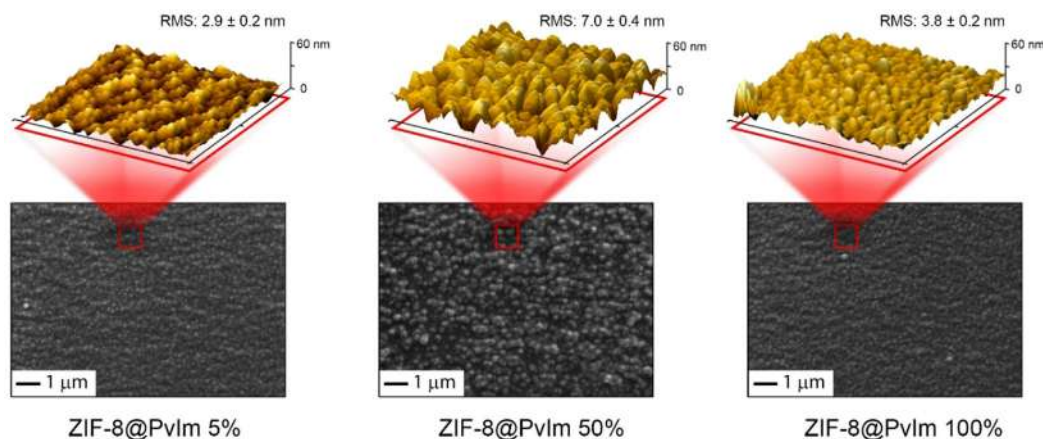
**Figure 2.** (a) ZIF-8@PvIm diffractograms obtained using different 3D primer grafting densities. Dashed lines correspond to the calculated XRD pattern. (b) Left axis: Frequency decrease ( $n = 3$  overtone) after completion of one cycle of ZIF-8 synthesis on polymer brushes grafted surfaces using different silanization mixtures (APTES percentage, x-axis). Right axis: Surface Mass Density ( $\Gamma$ ) obtained from the Sauerbrey equation. The dashed line corresponds to the non-specific deposition of ZIF-8 on 100% TEES silanized surface.

elastic solid.<sup>[55]</sup> The values obtained for  $\Gamma$  corresponding to films grown on grafted QCM sensors were compared to those from a control experiment conducted using a 100% TEES silanization mixture (i.e., no brush present) in order to take into account the contribution of non-specific ZIF-8 deposition (see Figure 2b).

#### Characterization of PvIm grafted substrates and ZIF-8@PvIm films

The surface morphology of PvIm grafted substrates was analyzed via AFM experiments (see Supporting Information, Section S2.3, and Figure S9); and the (APTES:TEES) ratio used in the silanization procedure was found to play a decisive role in

## a) ZIF-8@PvIm for different grafting densities:



## b) Non-specific deposition of ZIF-8:

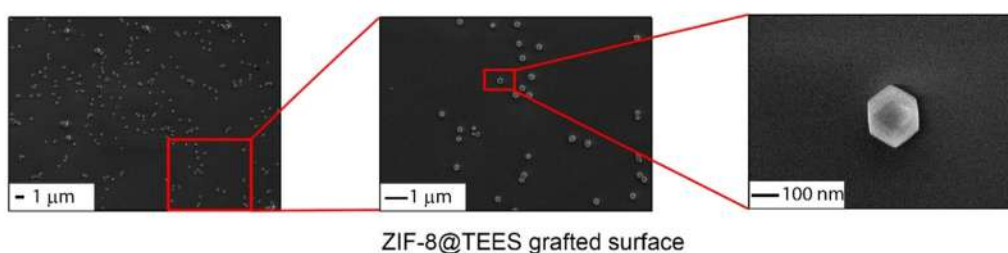


**Figure 3.** (a) Three-dimensional topographic images ( $1\ \mu\text{m} \times 1\ \mu\text{m}$ ) for ZIF-8@PvIm films with different APTES % grafting together with 25k magnification SEM images. (b) SEM images for non-specific deposition of ZIF-8 at increasingly higher magnification (from left to right).

3D primer structure (the morphologies obtained are quite different, as observed via SEM, see Figure S10 in the Supporting Information). Grafting density determines the average distance between polymer chains and density of exposed moieties involved in ZIF-8 nucleation; which ultimately affects the packing of film units related to the resulting constructional porosity (e.g., 50% grafting condition causes the polymer chains to present a topologically smoother surface than that obtained using 5% and 100%, as observed via AFM, see Supporting Information Figure S9). Film morphologies cannot be directly assessed from the roughness of the initial 3D primer as determined by AFM. Both AFM and SEM experiments were employed to gain further insight in this regard, see Figure 3a. For all the explored grafting densities, ZIF-8 MOF surface coverage can be assumed to be complete and different from what is observed when experiments are conducted using a 100% TEES-functionalized substrate surface (i.e., dispersed, non-specifically attached particles, rather than uniform films) see Figure 3b.

X-ray reflectometry (XRR) and Spectroscopic Ellipsometry (SE) techniques were employed to further characterize the architecture and lateral structure of composite films. The presence of multiple critical angles ( $\theta_c$ ) in XRR depends on the stratification and smoothness of the interphases between layers with different electronic densities. Specifically,  $\theta_c$  at  $q = 0.020 \pm 0.002\ \text{\AA}^{-1}$ , present in all the analyzed films, can be ascribed to ZIF-8 phase, while  $\theta_c$  at  $q = 0.031 \pm 0.002\ \text{\AA}^{-1}$  corresponds to Si substrates (see Figure 4a). Considering surface

roughness of films determined via AFM (see above), the intensity loss on XRR signal observed in films grown using 50% grafting density can be rationalized in terms of the damping produced by such local roughness. From the observed low-frequency Kiessig fringes (Kf), the presence of a thin layer of  $\Delta q = 0.08\ \text{\AA}^{-1}$ , equivalent to 8 nm thickness can be inferred. XRR experiments performed after ZIF-8 growth feature an additional critical angle, which suggests further stratification. In particular, for films obtained using 5% grafting density, high-frequency Kf are present (denoted with asterisks in Figure 4a). The spacing between Kf can be estimated to be  $\Delta q = 0.006 \pm 0.002\ \text{\AA}^{-1}$  equivalent to approx. 100 nm thickness, as expected for ZIF-8 films. Figure 4-b shows a comparison between XRR experiments carried over bare polymer brush (5% grafting density) before and after ZIF-8 synthesis. While  $\theta_c$  at  $q = 0.020 \pm 0.002\ \text{\AA}^{-1}$  corresponding to ZIF-8 is only present after film formation, the above-discussed low-frequency Kf appears in both experiments, thus supporting the above discussed proposed structure.

Spectroscopic Ellipsometry (SE) experiments were performed on ZIF-8@PvIm films using results obtained from XRR as input in the construction of a suitable model for interpretation of the composite material. Since both PvIm and ZIF-8 can be considered as transparent in the spectral range employed, the ellipsometry model was built using a combination of Cauchy layers. Table 2 summarizes the characteristic values for refractive index  $n$  and extinction coefficient  $k$ , after modelling exper-

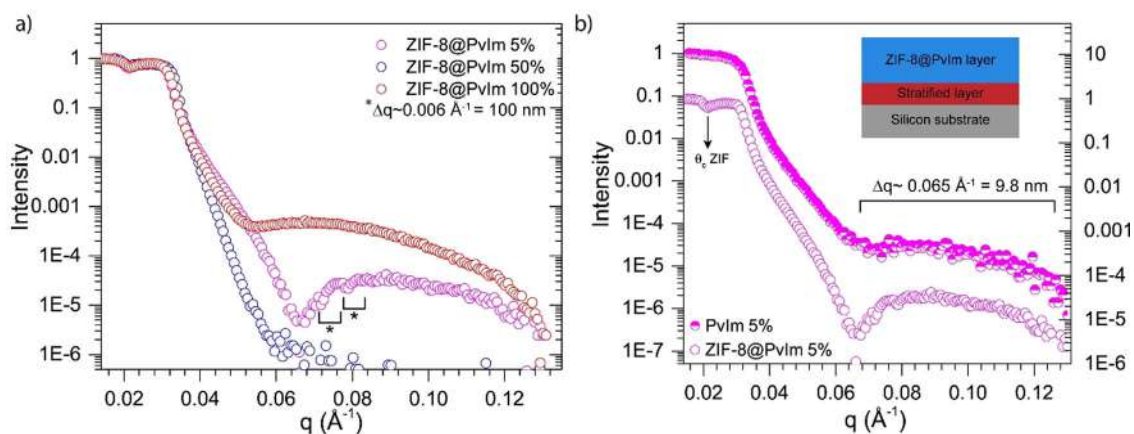


**Figure 4.** X-ray Reflectivity curves for (a) ZIF-8@PvIm at different grafting densities and (b) comparison between PvIm and ZIF-8@PvIm with 5% grafted surface. While normalized, the curves were plotted on separate axes for clarity purposes. \*Modulated high-frequency K $\alpha$ , see main text.

ZIF-8@PvIm X%	100	50	5
Stratified layer thickness [nm]	6.4	12.5	5.8
ZIF-8 layer thickness [nm]	111.8	119.3	126.1
Final Roughness [nm]	7.6	16.1	21.3
$n_{\text{ZIF-8}}^{\text{effective}}$ $\lambda=632.8 \text{ nm}$	1.3414	1.3436	1.3441
$k_{\text{ZIF-8}}^{\text{effective}}$ $\lambda=632.8 \text{ nm}$	0.0072	0.0077	0.0102
$\Gamma_{\text{ZIF-8}}^{\text{QCM}}$ [ $\mu\text{g cm}^{-2}$ ]	12.00	10.40	7.10

imental results obtained for films synthesized using different grafting density. Optical constants for ZIF-8@PvIm samples were fitted and compared with pure ZIF-8 films (high optical quality 608 nm thick ZIF-8 films were obtained using 3-mercapto-propane-sulfonic acid MPSA-modified gold substrates).<sup>[23]</sup> For further details on SE experiments and the use of pure ZIF-8 film reference, see section S2.4 in Supporting Information.

While the QCM-derived  $\Gamma$  shows that lower grafting densities imply less ZIF-8 being growth, SE experiments suggest that film thickness increases, as well as its surface roughness. This comparison suggests that lower packing densities arise from the use of lower PvIm grafting densities, thus affecting constructional porosity of the film.

### Different porous environments present on ZIF-8@PvIm films and the effect on adsorption properties

In order to characterize different porous environments, present in the films, SE experiments were performed in a flow cell alternating pure N<sub>2</sub>, methanol-saturated N<sub>2</sub>, and water-saturated N<sub>2</sub> streams. By carefully choosing the adsorbates, it is possible to explore the total or partial pore volume available for a given guest adsorbate; e.g., microporous volume present can be probed via methanol adsorption but is not available for water adsorption, while constructional porosity can be ac-

cessed by both adsorbates.<sup>[56]</sup> The measured changes on the Refractive Index (RI) after exposure to different adsorbates (flow conditions, 1.5 h equilibration time) can be related to pore-filling, as presented in Figure 5. The reversibility of the for adsorption/desorption cycles along with the stability of composite films can be inferred from almost constant optical surface mass density  $\Gamma_{\text{optical}}$ , which can be proved to be proportional to the product of layer thickness ( $d_{\text{ZIF}}$ ) and the solid volume fraction as obtained from Bruggeman's Effective Medium Approximation ( $f_{\text{ZIF}}$ )  $d_{\text{ZIF}} \times f_{\text{ZIF}}$ , as shown in Figure 5 inset.

Bruggeman approximation can be used to quantify film porosity in terms of volume fractions corresponding to both inherent ZIF-8 microporosity and interparticle constructional porosity. A detailed discussion on the assumptions made for calculations, along with a summary of the RI values obtained for different conditions can be found in Supporting Information, Tables S2 and S3. Briefly, Bruggeman approximation considers

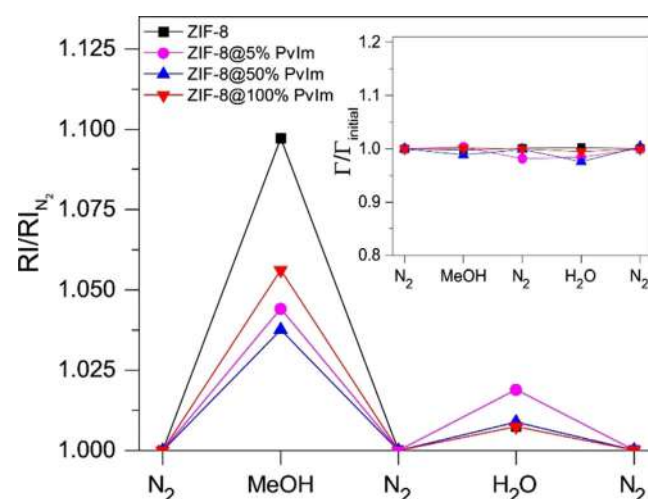


**Figure 5.** Relative refractive index measured at  $\lambda=632.8 \text{ nm}$  after exposure to different adsorbates in SE flow cell. Inset: Relative changes on optical Surface Mass Density according to Bruggeman approximation demonstrating the reversibility of the adsorption process.

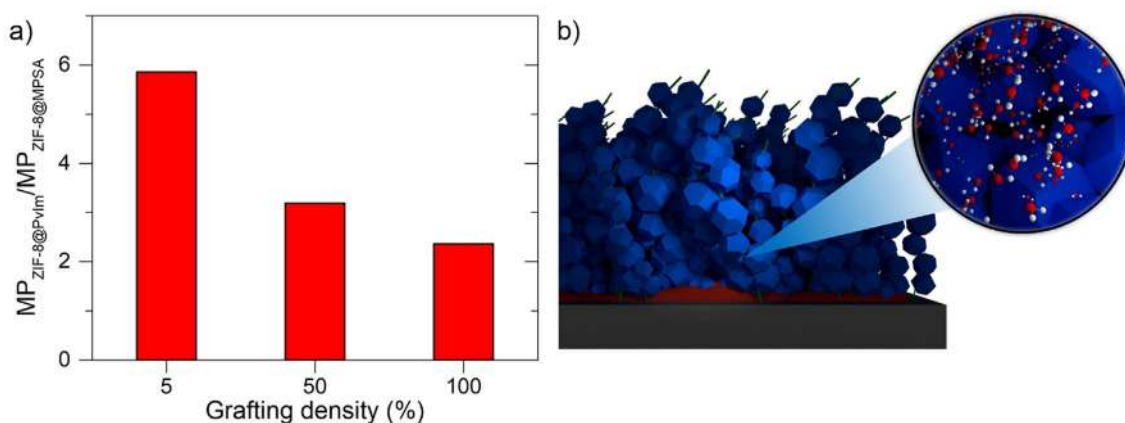


**Figure 6.** (a) Constructional interparticle porosity (MP) corresponding to ZIF-8@PvIm films relative to values measured for ZIF-8 films grown over MPSA self-assembled monolayers (calculated using Bruggeman approximation). (b) Schematic of mesoscopic domains generated by different grafting densities of polymer brushes defects on the resulting composite film.

a set of non-uniform inclusions into a continuous phase, allowing the deconvolution of individual contributions arising from each component (i.e., solid phase and empty or solvent-filled inclusions) to the final effective optical properties.

As shown in Figure 5, it is not possible to derive a straightforward dependence between relative variations on effective RI and grafting density after methanol exposure; e.g., films grown on 5% primer grafting density present a higher relative variation than 50% grafting density. Bruggeman approximation-based calculations allow rationalizing such observation since a lower total porosity was found for the films grown using a 50% grafting density than for those grown using a 5% grafting density (see Table S3 at Supporting Information). However, regarding water adsorption the trend observed is clear: as grafting density decreases, there is an increase in RI changes. Considering that (i) the available pore volume can be divided into microporosity (accessible only to  $N_2$  and methanol), and interparticle constructional porosity (mesoporosity MP, also accessible to water) and (ii) that after water adsorption, micropores remain totally filled with  $N_2$ ; it is possible to deconvolute the fraction corresponding to each contribution to the overall porosity available in the synthesized films, see Figure 6a. Values are presented as relative MP compared to the measured MP for ZIF-8@MPSA films in order to address the effect of polymer chains on the film structure (full details of calculation can be found in Supporting Information, see Table S3).

As can be seen, as grafting density decreases, MP increases. In other words, higher grafting densities result in more compact structures, while lower grafting density, generates increasingly inhomogeneous films with a higher proportion of interparticle constructional porosity.

## Conclusions

The strategy proposed for achieving a hierarchical structure of porous films relies on the control of spacing between surface-grafted poly(1-vinylimidazole) chains (3D primers), capable of  $Zn^{2+}$  preconcentration. This effect triggers the confined hetero-

ogeneous nucleation of ZIF-8 MOF. Through QCM experiments, it was demonstrated that the extent of MOF growth can be controlled by modifying brush grafting density; thus, evidencing the key role of PvIm chains for the nucleation and growth processes. Concomitantly, grafting density modulates the constructional porosity of the films obtained; increasing the surface density of brush-grafted chains, decreases the proportion of such mesoscopic pore space.

The results presented herein open the path to new strategies towards the rational design of hierarchically porous structures with different affinities in terms of hydrophilic character. The above-described synthesis strategy can be easily adapted to different MOFs by using suitable monomers for polymeric brush synthesis.

## Experimental Section

**Materials:** Silicon <100> wafers were purchased from PhotonExport. (3-aminopropyl)triethoxysilane (APTES), Triethoxy(ethyl)silane (TEES), alpha-bromoisobutyl bromide (Br-*i*BuBr), Triethylamine (TEA), Tetrahydrofuran (THF), anhydrous methanol, 1-vinylimidazole (vIm), Copper (I) Chloride, 2,2'-Bipyridil (Bpy), Ethylenediaminetetraacetic acid disodium salt dihydrate (EDTA), Zinc Nitrate Hexahydrate (ZnN), and 2-methylimidazole (HmIm), were purchased from Sigma-Aldrich and used without further purification. 5 MHz  $SiO_2$ -coated Quartz-Crystal Microbalance sensors were purchased from QuartzPro.

**Characterization methods:** X-ray Photoelectron Spectroscopy (XPS), Atomic Force Microscopy (AFM), Quartz-Crystal Microbalance (QCM), X-Ray Diffraction (XRD), X-Ray Reflectivity (XRR), Spectroscopic Ellipsometry (SE), Nuclear Magnetic Resonance (NMR), Fourier-Transform Infrared Spectroscopy (FTIR), and Scanning Electron Microscopy (SEM) were employed for characterization. Details on the experimental conditions applied can be found in the provided Supplementary Information file.

**Synthesis of ZIF-8@PvIm:** ATRP-synthesized Poly(1-vinylimidazole) brushes were used as 3D primers for ZIF-8 film growth; such films will be referred to ZIF-8@PvIm. The procedure followed is depicted in Scheme 1 (see detailed description in Supporting Information file) and can be briefly described in three consecutive steps: (i) both silicon slides and  $SiO_2$ -coated QCM substrates were modi-

fied with different APTES:TEES proportions (5–50–100% APTES content) by using a 2%v/v silane ethanolic solution at room temperature. Br-*i*BuBr ATRP initiator was then covalently bonded to APTES termination moieties by immersing the substrates into TEA/superdry toluene mixture and adding the initiator from a 20%v/v toluene solution for 24 h. (ii) Poly(1-vinylimidazole) brushes were grown by Cu-Bpy catalyzed ATRP reaction by immersing the functionalized substrates in a 0.15 g mL<sup>-1</sup> monomer solution. (iii) ZIF-8 films were grown by first exposing brush-grafted substrates to Zn<sup>2+</sup> methanolic solution in order to favor the preconcentration of metal ions via coordination with imidazole moieties on the polymer brush. Then, 2-methylimidazole (Hmlm) methanolic solution was added with the ZIF-8 stoichiometric molar ratio, and the reaction was conducted for 30 min, followed by substrate washing with fresh solvent and drying.

## Acknowledgements

M.R., J.M.G., M.C., C.v.B., and O.A. are CONICET staff members. J.A.A. and A.I. want to acknowledge CONICET for a doctoral scholarship. Financial support from Universidad Nacional de La Plata (Project PPIID/X026) and Agencia Nacional de Promoción Científica y Tecnológica (ANPCyT, PICT-2018-00780) is gratefully acknowledged. S.M. thanks the MAT2017-88752-R2017 Retos project from the Spanish Ministry of Economics.

## Conflict of interest

The authors declare no conflict of interest.

**Keywords:** constructional porosity · mesoporous materials · metal–organic frameworks · microporous materials · polymer brushes · ZIF-8

- [1] T. J. Barton, L. M. Bull, W. G. Klemperer, D. A. Loy, B. McEnaney, M. Misono, P. A. Monson, G. Pez, G. W. Scherer, J. C. Vartuli, O. M. Yaghi, *Chem. Mater.* **1999**, *11*, 2633–2656.
- [2] P. Innocenzi, L. Malfatti, G. J. A. A. A. Soler-Illia, *Chem. Mater.* **2011**, *23*, 2501–2509.
- [3] C. M. A. Parlett, K. Wilson, A. F. Lee, *Chem. Soc. Rev.* **2013**, *42*, 3876–3893.
- [4] Y. Li, Z. Y. Fu, B. L. Su, *Adv. Funct. Mater.* **2012**, *22*, 4634–4667.
- [5] L. Deliere, F. Villemot, D. Farrusseng, A. Galarneau, S. Topin, B. Coasne, *Microporous Mesoporous Mater.* **2016**, *229*, 145–154.
- [6] H. Furukawa, N. Ko, Y. B. Go, N. Aratani, S. B. Choi, E. Choi, A. O. Yazaydin, R. Q. Snurr, M. O’Keeffe, J. Kim, O. M. Yaghi, *Science* **2010**, *329*, 424–428.
- [7] P. Falcaro, R. Ricco, C. M. Doherty, K. Liang, A. J. Hill, M. J. Styles, *Chem. Soc. Rev.* **2014**, *43*, 5513–5560.
- [8] B. F. Hoskins, R. Robson, *J. Am. Chem. Soc.* **1989**, *111*, 5962–5964.
- [9] H. Li, M. Eddaoudi, M. O’Keeffe, O. M. Yaghi, *Nature* **1999**, *402*, 276–279.
- [10] A. Zimpel, N. Al Danaf, B. Steinborn, J. Kuhn, M. Höhn, T. Bauer, P. Hirschle, W. Schimpf, H. Engelke, E. Wagner, M. Barz, D. C. Lamb, U. Lächelt, S. Wuttke, *ACS Nano* **2019**, *13*, 3884–3895.
- [11] T. Rijnaarts, R. Mejia-Ariza, R. J. M. Egberink, W. Vanroosmalen, J. Huskens, *Chem. Eur. J.* **2015**, *21*, 10296–10301.
- [12] D. Yang, V. Bernaldes, T. Islamoglu, O. K. Farha, J. T. Hupp, C. J. Cramer, L. Gagliardi, B. C. Gates, *J. Am. Chem. Soc.* **2016**, *138*, 15189–15196.
- [13] Y. Sun, Q. Sun, H. Huang, B. Aguila, Z. Niu, J. A. Perman, S. Ma, J. Mater. Chem. A **2017**, *5*, 18770–18776.
- [14] M. J. Van Vleet, T. Weng, X. Li, J. R. Schmidt, *Chem. Rev.* **2018**, *118*, 3681–3721.
- [15] Z. Fu, G. Xu, *Chem. Rec.* **2017**, *17*, 518–534.
- [16] B. Liu, R. A. Fischer, *Sci. China Chem.* **2011**, *54*, 1851–1866.
- [17] D. Zacher, R. Schmid, C. Wöll, R. A. Fischer, *Angew. Chem. Int. Ed.* **2011**, *50*, 176–199; *Angew. Chem.* **2011**, *123*, 184–208.
- [18] A. Bétard, R. A. Fischer, *Chem. Rev.* **2012**, *112*, 1055–1083.
- [19] J. Liu, O. Shekha, X. Stammer, H. K. Arslan, B. Liu, B. Schüpbach, A. Terfort, C. Wöll, *Materials* **2012**, *5*, 1581–1592.
- [20] C. Hou, Q. Xu, J. Peng, Z. Ji, X. Hu, *ChemPhysChem* **2013**, *14*, 140–144.
- [21] K. Kida, K. Fujita, T. Shimada, S. Tanaka, Y. Miyake, *Dalton Trans.* **2013**, *42*, 11128–11135.
- [22] J. S. Tuninetti, M. Rafti, O. Azzaroni, *RSC Adv.* **2015**, *5*, 73958–73962.
- [23] J. A. Allegretto, J. Dostalek, M. Rafti, B. Menges, O. Azzaroni, W. Knoll, *J. Phys. Chem. A* **2019**, *123*, 1100–1109.
- [24] S. Qiu, M. Xue, G. Zhu, *Chem. Soc. Rev.* **2014**, *43*, 6116–6140.
- [25] V. Rubio-Giménez, S. Tatay, F. Volatron, F. J. Martínez-Casado, C. Martí-Gastaldo, E. Coronado, *J. Am. Chem. Soc.* **2016**, *138*, 2576–2584.
- [26] S. Wannapaiboon, M. Tu, K. Sumida, K. Khaletskaia, S. Furukawa, S. Kitagawa, R. A. Fischer, *J. Mater. Chem. A* **2015**, *3*, 23385–23394.
- [27] J. Liu, C. Wöll, *Chem. Soc. Rev.* **2017**, *46*, 5730–5770.
- [28] C. Zhu, J. A. Perman, R. E. Gerald, S. Ma, J. Huang, *ACS Appl. Mater. Interfaces* **2019**, *11*, 4393–4398.
- [29] K. Xie, Q. Fu, P. A. Webley, G. G. Qiao, *Angew. Chem. Int. Ed.* **2018**, *57*, 8597–8602; *Angew. Chem.* **2018**, *130*, 8733–8738.
- [30] N. A. H. M. Nordin, A. F. Ismail, A. Mustafa, R. S. Murali, T. Matsuura, *RSC Adv.* **2014**, *4*, 52530–52541.
- [31] Z. Li, Y. Guo, X. Wang, W. Ying, D. Chen, X. Ma, X. Zhao, X. Peng, *Chem. Commun.* **2018**, *54*, 13865–13868.
- [32] G. E. Fenoy, J. Scotto, J. Azcárate, M. Rafti, W. A. Marmisollé, O. Azzaroni, *ACS Appl. Energy Mater.* **2018**, *1*, 5428–5436.
- [33] M. I. Velasco, R. H. Acosta, W. A. Marmisollé, O. Azzaroni, M. Rafti, *J. Phys. Chem. C* **2019**, *123*, 21076–21082.
- [34] Z. Zhang, H. T. H. Nguyen, S. A. Miller, S. M. Cohen, *Angew. Chem. Int. Ed.* **2015**, *54*, 6152–6157; *Angew. Chem.* **2015**, *127*, 6250–6255.
- [35] A. Carné-Sánchez, K. C. Stylianou, C. Carbonell, M. Naderi, I. Imaz, D. Maspocho, *Adv. Mater.* **2015**, *27*, 869–873.
- [36] H. Sun, B. Tang, P. Wu, *ACS Appl. Mater. Interfaces* **2017**, *9*, 21473–21484.
- [37] S. Dong, Q. Chen, W. Li, Z. Jiang, J. Ma, H. Gao, *J. Mater. Chem. B* **2017**, *5*, 8322–8329.
- [38] K. A. McDonald, J. I. Feldblyum, K. Koh, A. G. Wong-Foy, A. J. Matzger, *Chem. Commun.* **2015**, *51*, 11994–11996.
- [39] S. He, H. Wang, C. Zhang, S. Zhang, Y. Yu, Y. Lee, T. Li, *Chem. Sci.* **2019**, *10*, 1816–1822.
- [40] J.-L. Zhuang, A. Terfort, C. Wöll, *Coord. Chem. Rev.* **2016**, *307*, 391–424.
- [41] R. Zhang, S. Ji, N. Wang, L. Wang, G. Zhang, J.-R. Li, *Angew. Chem. Int. Ed.* **2014**, *53*, 9775–9779; *Angew. Chem.* **2014**, *126*, 9933–9937.
- [42] M. Rafti, J. A. Allegretto, G. M. Segovia, J. S. Tuninetti, J. M. Giusti, E. Bindini, O. Azzaroni, *Mater. Chem. Front.* **2017**, *1*, 2256–2260.
- [43] L. Hou, M. Zhou, X. Dong, L. Wang, Z. Xie, D. Dong, N. Zhang, *Chem. Eur. J.* **2017**, *23*, 13337–13341.
- [44] M. Eddaoudi, D. F. Sava, J. F. Eubank, K. Adil, V. Guillerme, *Chem. Soc. Rev.* **2015**, *44*, 228–249.
- [45] K. S. Park, Z. Ni, A. P. Cote, J. Y. Choi, R. Huang, F. J. Uribe-Romo, H. K. Chae, M. O’Keeffe, O. M. Yaghi, *Proc. Natl. Acad. Sci. USA* **2006**, *103*, 10186–10191.
- [46] M. J. Lee, H. T. Kwon, H.-K. Jeong, *J. Membr. Sci.* **2017**, *529*, 105–113.
- [47] D. Cunha, M. Ben Yahia, S. Hall, S. R. Miller, H. Chevreau, E. Elkaim, G. Maurin, P. Horcajada, C. Serre, *Chem. Mater.* **2013**, *25*, 2767–2776.
- [48] G. Lu, J. T. Hupp, *J. Am. Chem. Soc.* **2010**, *132*, 7832–7833.
- [49] S. Eslava, L. Zhang, S. Esconjauregui, J. Yang, K. Vanstreels, M. R. Baklanov, E. Saiz, *Chem. Mater.* **2013**, *25*, 27–33.
- [50] G. Lu, O. K. Farha, W. Zhang, F. Huo, J. T. Hupp, *Adv. Mater.* **2012**, *24*, 3970–3974.
- [51] B. L. Rivas, H. A. Maturana, M. J. Molina, M. R. Gomez-Aanton, I. F. Pierola, *J. Appl. Polym. Sci.* **1998**, *67*, 1109–1118.
- [52] S. Tugulu, R. Barbey, M. Harms, M. Fricke, D. Volkmer, A. Rossi, H.-A. Klok, *Macromolecules* **2007**, *40*, 168–177.

- [53] X. Luo, S. H. Goh, S. Y. Lee, C. H. A. Huan, *Macromol. Chem. Phys.* **1999**, *200*, 874–880.
- [54] R. L. Papporello, E. E. Miró, J. M. Zamaro, *Microporous Mesoporous Mater.* **2015**, *211*, 64–72.
- [55] B. D. Vogt, E. K. Lin, W. Wu, C. C. White, *J. Phys. Chem. B* **2004**, *108*, 12685–12690.
- [56] K. Zhang, R. P. Lively, C. Zhang, W. J. Koros, R. R. Chance, *J. Phys. Chem. C* **2013**, *117*, 7214–7225.

---

Manuscript received: May 20, 2020

Accepted manuscript online: July 16, 2020

Version of record online: ■ ■ ■, 0000

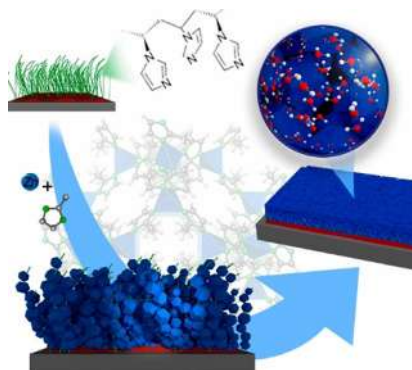
## FULL PAPER

### Porous Materials

*J. A. Allegretto, A. Iborra, J. M. Giusi,  
C. von Bilderling, M. Ceolín, S. Moya,  
O. Azzaroni,\* M. Rafti\**



### Growth of ZIF-8 MOF Films with Tunable Porosity by using Poly (1-vinylimidazole) Brushes as 3D Primers



**Poly(1-vinylimidazole) brushes** served as heterogeneous nucleation points for ZIF-8 MOF growth. By modifying the brush grafting density, the films featured inherently hydrophobic microporosity arising from ZIF-8 structure, and an additional constructional interparticle mesoporosity, which can be employed for differential adsorption of targeted adsorbates.